Convolutional Neural Networks For Apical Lesion Segmentation From Panoramic Radiographs

Il-Seok Song
Seoul National University
Hak-Kyun Shin
AI Research Center of DDH Incorporation
Ju-Hee Kang
Seoul National University
Jo-Eun Kim
Seoul National University
Kyung-Hoe Huh
Seoul National University
Won-Jin Yi
Seoul National University
Sam-Sun Lee
Seoul National University
Min-Suk Heo (hmslsh@snu.ac.kr)
Seoul National University

Research Article

Keywords: Convolutional neural network, artificial intelligence, panoramic radiographs, dental researches

Posted Date: November 8th, 2021

DOI: https://doi.org/10.21203/rs.3.rs-1018527/v1

Abstract

Convolutional neural networks (CNNs) have rapidly emerged as one of the most promising next-generation artificial intelligence (AI) in the field of medical and dental researches, which can further provide an effective diagnostic methodology allowing for detection of diseases at early age. This study was, thus, aimed to evaluate performances for apical lesion segmentation from panoramic radiographs using two CNN algorithms including U-Net and FPN. A total of 1000 panoramic radiographs showing apical lesions were separated into training (n = 800, 80%), validation (n = 100, 10%), and test (n = 100, 10%) dataset, respectively. These datasets were further incorporated to construct CNN models using two algorithms, respectively. The performances of identifying apical lesions were evaluated after calculating precision, recall, and F1-score from both CNN models. Both U-Net and FPN algorithms provided considerably good performances in identifying apical lesions in panoramic radiographs.

Introduction

Apical periodontitis is an inflammatory disease of peri-radicular tissues derived from constant microbial infection within the root canal of the tooth.[1] The infected and necrotic pulp provides a habitat for the organisms.[2] The microbes develop in sessile biofilms, aggregates, and also as planktonic cells suspended in the aqueous phase of the canal.[3] A biofilm is a colony of microorganisms embedded in an exopolysaccharide matrix that attaches to a wet surface, but planktonic organisms are floating single microbial cells in an fluidic environment.[4] Microorganisms covered by biofilms are higher than one thousand times more resistant to biocides as the same organisms in planktonic form.[5,6]

Apical periodontitis is identified radiographically as apical radiolucencies. When a periapical lesion communicates with a deep periodontal pocket, apical lesions develop into the endodontic-periodontic lesions with J-shaped radiolucencies. Those radiolucencies may be identified by a targeted radiographic examination. However, in most cases, apical lesions are detected from radiographic images taken for other reason by chance.

Regardless of their distinguishable ability, radiographic examinations are prone to suffering from inter- and intra-examiner reliability.[7,8] This reliability further depends on the experience of trained examiner.[9] Current empirical approaches for medical and dental prediction and analysis of quantitative and qualitative dental disease, therefore, heavily relies on the combination of experience and subjective evaluation of the dental specialists. Such clinical approaches and methodologies are inefficient in achieving early detection and accurate prediction of dental disease as entirely dominated by a large amount of time and effort in the screening processes. These are further limited in their ability to provide more reliable and standard clinical evaluation. For instance, in the field of radiographic imaging, the detection of landmarks in cephalograms, detection of maxillary sinusitis, and early-stage diagnosis of dental caries and periodontitis heavily required for significantly time-consuming process involving an interconnected small unit of detection tasks which are also mostly performed through evaluation of human labors.

With the aid of recently emerging artificial intelligence, the deep-learning (defined as a subset of machine learning) guided recognition has successfully demonstrated its excellent ability and performance in the field of medical and dental applications.[10,11] The inherent problem in the empirical approaches can be efficiently overcome particularly in the oral and maxillofacial imaging through deep-learning approaches to classify, convert 2-dimensional panoramic radiographs, and simultaneously diagnose the diseases in the converted radiographs.[12]

This study performed convolutional neural networks (CNN)-based approaches aiming for identifying apical lesions on panoramic radiograph. Rather than relying on manually cropped image segment of each tooth as the initial training datasets,[13] our study employing the entire panoramic image as a training dataset can provide a screening and detecting early-staged apical lesions efficiently. The rapid screening and automatic prediction of the dental diseases enabled by the deep learning processes allows for facilitating more efficient diagnosis and rapid detection for apical lesions with high precision and sensitivity. The novel deep-learning approaches and frameworks developed in this study provide a fundamental insight into more efficient detection and classification of dental diseases with data augmentation, which can be also applied in other medical fields.

Two CNNs including U-Net and Feature Pyramid Network (FPN) were adopted for apical lesion segmentation in this study. Previous studies adopted YOLO network for detecting dental diseases.[14,15] Semantic segmentation is a form of pixel-level prediction and seemed more appropriate for identifying apical lesions with small pixels. Two representative networks are U-Net and FPN for semantic segmentation.[16]

The purpose of this study was to evaluate performances for apical lesion segmentation from panoramic radiographs using two CNN algorithms including U-Net and FPN.

Results

This study was designed to evaluate and compare the performances using two different CNN models through deep learning assisted algorithms including U-Net and FPN on how they effectively and efficiently detected and diagnosed apical lesions on panoramic radiograph. The specific detection performances of each model (U-Net versus FPN) were evaluated by computing precision, recall and F1-score values, respectively, as summarized in Table 1. As demonstrated in experimental section, the precision value is the primarily important parameter to be considered for detecting performances.

Table 1
Precision (positive predictive value), recall (sensitivity), and F1-score for the detection of apical lesions of the U-Net and FPN.

IoU Threshold	U-Net			FPN		
	Precision	Recall	F1-score	Precision	Recall	F1-score
0.01	0.875	0.855	0.864	0.841	0.865	0.853
0.1	0.869	0.850	0.859	0.836	0.858	0.847
0.3	0.830	0.801	0.815	0.817	0.825	0.821
0.5	0.731	0.698	0.714	0.716	0.719	0.718

When panoramic radiographs were filtered out the by adjusting the threshold of intersection over union (IoU) from 0.01-0.5, the detection performances were evaluated for two CNN models. In both models, all of the detection performances (precision, recall, and F1-score) generally decreased from 0.841-0.875 (at IoU of 0.01) to 0.698-0.731 (at IoU of 0.5) with gradually increasing the IoU threshold intensity. Taking into account of F1-score calculated from reflecting both precision and recall parameters, the increased F1-score with smaller IoU threshold further suggested that detection and classification performances are improved. Fig. 3 shows the graphs corresponding these data.

When the performances of U-Net were compared with analogues of FPN at different IoU threshold (0.01-0.5), all of performances corresponding to U-Net showed higher values (and better performances) than those of FPN. The performance values were 0.875, 0.855, and 0.864, respectively, for U-Net model corresponding to precision, recall, and F1-score from former to latter at the lowest IoU threshold of 0.01 whereas the corresponding values for FPN are 0.841, 0.865, 0.853, respectively. Even at the higher IoU thresholds in the range of 0.1, similar data trend was also observed as well. The F1-score (average value of precision and recall) was 0.859 for U-Net and 0.847 for FPN at 0.1. Even at the higher IoU threshold in the range of 0.3-0.5, similar performance values for U-Net and FPN were observed.

Figure 4a shows a panoramic radiograph image corresponding to training dataset in U-Net models (as demonstrated in Fig. 1) for classifying and detecting apical lesion. Red and yellow areas represent the labeling of the selected area for segmentation. Fig. 4b corresponds to the intensity histogram of the images shown in the panel of Figure 4a as a function of number of a specific pixel. During the image processing, the intensity histogram of an images is generated through converting the images with 256 numbers of pixel distribution based on those grayscale values (lower number of pixel reflects the darker images and higher number of pixel corresponds to lighter images). In this histogram, the pixel numbers in the pixel ranges of 81-91 showed the highest probable density populations found in that image of Figure 4a.

Figure 5 represent relative comparison between the training (red line) and validation (blue line) with pretrained augmented models using U-Net algorithm developed in Fig. 1. The training and validation datasets were evaluated over the course of each epoch from 0-450 and each epoch represent one pass

through the entire training dataset. The loss (or accuracy in reverse) recorded for training and validation dataset generally decreased during the course of repeated 450 epochs. The final resulting loss value was 0.30 for validation and 0.18 for training dataset. Both losses flattened out after 400 epochs, implying no additional improvement made after this epoch.

Figure 6 depicts the panoramic radiographic images corresponding to apical lesion segmentation as a function of utilizing U-Net and FPN CNN-based learning. Original images were preprocessed with specific selection of area for examining the diagnostic apical lesion. In Fig. 6, green areas indicate the manual labeling from dental specialist with expertise in this field more than 10 years. The yellow areas correspond to the U-Net models-guided labeling (Fig. 6c,6d) and the red areas correspond to the FPN model-guided labeling (Fig. 6e,6f) for apical lesion. Both the labeling by U-Net and FPN were not significantly different from the manual labeling.

Discussion

Accurate and early detection of apical lesions is an important factor for preventing pain and simultaneously improving treatment prognosis.[17] When apical lesions cannot be diagnosed at the early stage, the lesions may grow progressively inducing pain, swelling, and bone loss around the apex, which ultimately leads to loss of tooth. Various imaging modalities can be employed for detecting apical lesions. Among them, the panoramic radiography is the most frequently used for identifying dental diseases at the first visit because the apical lesions can be detected at early stage using panoramic radiographs. However, radiographic detection of apical lesions is not objective between examiners and detecting ability is heavily dependent on the experience and skill of highly trained examiners.

To date, a few studies have employed deep learning as a tool for detecting apical lesions. A deep learning-based CNN algorithm enabled the automated detection of apical lesions efficiently and effectively with minimizing the dependence on the ability of examiners. However, to the best our knowledge, no study has examined the functionality of CNN for automated diagnosis of apical lesions thus far using entire panoramic radiographs. In this study, panoramic radiographs were used for training to detect apical lesions and the possibility of AI-guided diagnosis of apical lesions at early stage was confirmed.

U-Net and FPN models were used to detect apical lesions. Both algorithms are representative models for semantic segmentation and showed relatively great performance enough for clinical applications. U-Net demonstrated overall detection performance of 0.875 of precision, 0.855 of recall, 0.864 of F1-score while FPN showed 0.841 of precision, 0.865 of recall, 0.853 of F1-score, respectively.

Data augmentation is commonly used in training CNN models.[15,18,19] It is an integral process of many state-of-the-art deep learning systems on image classification, object detection, and segmentation.[20] Current deep neural networks have a number of parameters, tending to overfit the limited training data. Data augmentation is used to increase both the quantity and diversity of training data, thus preventing

the overfitting and improving generalization.[21] In this study, online data augmentation was used. It can optimize data augmentation and target network training in an online manner. The merits of online augmentation is the opposite features of offline methods.[22] Their complementary character makes it possible to apply them together. The augmentation network can apply to the target network through online training from the start to finish excluding the inconveniences of pre-training or early stopping. Learning offline methods usually rely on distributed training, as there are many parallel optimization processes, but online data augmentation is simple and easy for training.

The performances were evaluated under even 0.01 of IoU value. In the most cases, the lesion area has a slight change in color or contrast in the panoramic radiographs and also can be observed as just a few pixels. Even if the lesion area and the CNN-predicted area match only a very small amount, it can be considered that the result is valid for this reason. Therefore, parameters for evaluating performances at the IoU value of 0.01 can be used as the performance index value of the CNN model in this study.

CNN-based models identified the apical lesions on maxilla and mandible with high performances, but it showed higher accuracy in the mandible than in the maxilla. Many anatomical structures such as sinus floor, nasal cavity, anterior nasal spine was superimposed and interfered the segmentation process of CNN. In contrast, there were not many overlapping anatomical structures on mandible, which indicated the better results.

Conclusion

The potential utility of deep learning for the detection and diagnosis of apical lesions was identified. Both U-Net and FPN algorithms provided considerably good performances in detecting apical lesions in panoramic radiographs. CNN-based diagnosis may be a competent assistant to detect dental and medical diseases at early stage.

Materials And Methods

Data preparation

The dataset consisted of a total of 1000 panoramic radiograph samples of patients who visited Seoul National University Dental Hospital during the period of time from 2018 to 2019. These radiographs included 1691 apical lesions. Panoramic radiographs were obtained from adult patients without mixed dentition, and only one radiograph was used per a single patient. Small apical lesions indistinguishable from periodontal ligament thickening were excluded. Lesions superimposed with maxillary sinus were excluded. Radiographic images with severe noise and blurring were also excluded. The study was approved by the Institutional Review Board (IRB) of Seoul National University Dental Hospital (ERI19010) with a waiver of informed consent. The data collection and all experiments were performed in accordance with the relevant guidelines and regulations.

Apical lesion labeling

Apical lesions were detected by three oral and maxillofacial radiologists. The lesion determined to be correct by two or more radiologists can be further treated as a gold standard. Panoramic radiographs had a resolution of 1976×976 pixels, and each radiograph was labeled manually in red by drawing outline of the lesions using polygon labeling tools for training. Not only apical lesions but also endodontic-periodontic lesions were labeled in yellow. Apical lesions and endodontic-periodontic lesions were trained together without distinction.

Preprocessing and augmentation of panoramic radiographs

A total of 1000 panoramic radiographs were collected and resized to 1280×768 pixels and converted into PNG file format. The datasets were randomly divided into training and validation sets (n = 903 [90%]), and a test dataset (n = 100 [10%]) before data augmentation. The training dataset was composed of 1691 apical lesions. The training dataset was randomly augmented during all phases using flip, blur, shift, scale, rotation, sharpening, emboss, contrast, brightness, grid distortion, and elastic transform through online augmentation. Online augmentation uses a specific augmentation method at each phase for optimized training, and it is transferable and more effective for models trained on limited training datasets.[23]

Architecture of the deep convolutional neural network algorithm

Two different CNNs models were used in this study; one was U-Net and the other was FPN. In the first CNN model, a pre-trained U-Net CNN network was used for preprocessing and transfer learning. Fig. 1 demonstrates a schematic illustration for CNNs based on U-Net model architecture.[24] In particular, the U-Net model is comprised of two different paths including a contracting path (left) and an expansive path (right). In the contracting part, the original radiographic images are used as input to encode for multiple layers of convolution (3x3), rectified linear unit (ReLU) activation, max-pooling operation (2x2), and compression into a latent space. At each contracting step, the number of feature channels were doubled. The expanding part is a reverse process of contracting part. Specifically, CNNs attempts to translate the contracted information from the latent space through upconvolution operation (2x2) with a feature map wherein the number of feature channels reduced to half and further to generate the segmentation mask of the image. The rest of the decoding operations is reverse of the encoding parts (cropping feature map from contracting path, 3x3 convolution, ReLU). Importantly, the cropping of images is necessarily required as a result of loss of information related to border pixels during the process of every convolution. For mapping 64-component feature vector to the desired number of classes, the last layer of a 1x1 convolution is finally utilized. In total, the network has 23 convolutional layers.

The other CNN model developed here in this study is the FPN to implement land segmentation. The general scheme for FPN is illustrated in Fig. 2. The FPN is comprised of two different processes including the bottom-up and top-down paths (as similar to contracting and expanding shown in the U-Net CNN).[25] As similar to U-Net architecture, the bottom-up process corresponds to the selection of features in the

convolutional neural network. In this FPN architecture, a pre-trained ResNet50 encoder were selected for feature extraction. This process involves many convolution modules with many convolution layers. The spatial dimension is decreased to half at each stage of the bottom-up process. The output of each convolution module is denoted by Ci and utilized in the top-down pathway later.

In the bottom-up pathway, the spatial resolution is reduced. The semantic value for each layer is increased with more high-level structures extracted. Conv1 occupies too much memory, so it is excluded. On the top of the bottom-up pathway, C5 channel depth is decreased to 256 to create M5 module using 1x1 convolution filter. Then 3x3 convolution is applied two times to create P5, which becomes the initial feature map layer used for segmentation. The P5 has the same spatial resolution as conv5 and 128 channels. Going down in the top-down pathway, the former layer is upsampled by 2 using nearest layers upsampling. 1x1 convolution is utilized to the equivalent feature maps in the bottom-up pathway again. Each element are concatenated. After then, 3x3 convolution is applied two times to output the following feature map layers for segmentation. This filter reduces the aliasing effect of upsampling.

In the last step, all Pi modules, which have 1/4 of the input image resolution and 128 channels, were combined to have a module with 512 channels. After that, 512 3x3 convolution filters, batch normalization, and ReLU activation is applied. As a next step, 1x1 convolutions is utilized to reduce the number of channels to get seven output channels. And then, spatial dropout operation is applied to upsample to the actual size by bi-linear interpolation.[26]

Evaluation of detection and classification performance of the deep CNN model

The performances of the developed CNN models were evaluated only using test datasets not determined from training datasets. Precision, recall, and F1-score were calculated as demonstrated in the following equations (1-3). These parameters were commonly calculated for evaluating performances of CNN models.

$$Precision = \frac{TP}{FP + TP} (1)$$

$$Recall = \frac{TP}{FN + TP} (2)$$

$$F1 - score = 2 \bullet \frac{Precision \bullet Recall}{Precision + Recall} (3)$$

where TP represents the true positive; FP represents the false positive; and FN represents the false negative.

Declarations

Data availability

Panoramic radiographs in dataset used for training, validation, and testing of this study are not publicly available due to the restriction by the Institutional Review Board (IRB) of Seoul National University Dental Hospital to protect patients' privacy.

Acknowledgements

This study was supported by grant (No. 04-2020-0106) from the SNUDH Research Fund, and this work was also supported by DDH Research Center grant funded by DDH Inc., South Korea.

Author contributions

I.S.: Contributed to conception and design, data acquisition, analysis and interpretation, and drafted and critically revised the manuscript. H.S.: Contributed to conception and design, data acquisition. J.K.: Contributed to conception and design, data interpretation. J.K.: Contributed to conception and design, data interpretation. K.H.: Contributed to conception and design, data interpretation, and drafted the manuscript. W.Y.: Contributed to conception and design, data interpretation, and drafted the manuscript. S.L.: Contributed to conception and design, data interpretation, and drafted the manuscript. M.H.: Contributed to conception and design, data acquisition, analysis and interpretation, and drafted and critically revised the manuscript. "All authors gave their final approval and agree to be accountable for all aspects of the work".

Competing interests

2nd author, Hak-Kyun Shin invented the AI software model (called Deep stack) and is still working for the company (DDH Inc., Seoul, South Korea) that developed it. The other authors have no conflict of interest to declare. The funders had no role in the design of the study; in the collection, analyses, or interpretation of data; in the writing of the manuscript, or in the decision to publish the results.

Additional information

Corresponding Author

* Corresponding author: Heo, M.S. (hmslsh@snu.ac.kr)

References

1. Kakehashi, S., Stanley, H.R., Fitzgerald, R.J. The effects of surgical exposures of dental pulps in germ-free and conventional laboratory rats. *Oral Surg. Oral Med. Oral Pathol.* **20**, 340-349 (1965).
2. Fabricius, L., Dahlén, G., Holm S.E., Möller, A.J. Influence of combinations of oral bacteria on periapical tissues of monkeys. *Scandi. J. Dent. Res*. **90**, 200-206 (1982).
3. Nair P.N.R. On the causes of persistent apical periodontitis: a review. *Int. Endod. J.* **39**, 249-281 (2006).

4. Costerton, W. et al. The application of biofilm science to the study and control of chronic bacterial infections. *J. Clin. Investig.* **112**, 1466-1477 (2003).
5. Wilson M. Susceptibility of oral bacterial biofilms to antimicrobial agents. *J. Med. Microbiol.* **44**, 79-87 (1996).
6. Costerton, J.W., Stewart, P.S. Biofilms and device-related infections. In: Nataro J.P., Blaser M.J., Cunningham-Rundles S., eds. *Persistent bacterial infections. Washington, DC: ASM Press*, 423-439 (2000).
7. Nardi, C. et al. Is panoramic radiography an accurate imaging technique for the detection of endodontically treated asymptomatic apical periodontitis? *J. Endodon.* **44,** 1500-1508 (2018).
8. Nardi, C. et al. Accuracy of orthopantomography for apical periodontitis without endodontic treatment. *J. Endodon.* **43**, 1640-1646 (2017).
9. Parker, J.M., Mol, A., Rivera, E.M., Tawil, P.Z. Cone-beam computed tomography uses in clinical endodontics: observer variability in detecting periapical lesions. *J. Endodon.* **43**, 184-187 (2017).
10. Nagi, R. et al. Clinical applications and performance of intelligent systems in dental and maxillofacial radiology: A review. *Imaging Sci Dent.* **50**, 81-92 (2020).
11. Hwang, J.J., Jung, Y.H., Cho, B.H., Heo, M.S. An overview of deep learning in the field of dentistry. *Imaging Sci Dent.* **49**, 1-7 (2019).
12. Schmidhuber, J. Deep learning in neural networks: an overview. *Neural Networks* **61**, 85-117 (2015).
13. Ekert, T. et al. Deep Learning for the Radiographic Detection of Apical Lesions. *J. Endodon.* **45**, 917-22 (2019).
14. Yüksel, A.E. et al. Dental enumeration and multiple treatment detection on panoramic X-rays using deep learning. *Sci. Rep.* **11**, 12342 (2021).
15. Kwon, O.D. et al. Automatic diagnosis for cysts and tumors of both jaws on panoramic radiographs using a deep convolution neural network. *Dentomaxillofac. Rad.* **49**; https://doi.org/10.1259/dmfr.20200185 (2020).
16. Qian K. Automated Detection of Steel Defects via Machine Learning Based on Real-Time Semantic Segmentation. *Proceedings of the 3rd International Conference on Video and Image Processing (ICVIP)* 42-46 (2019).
17. Abbott, P.V. Classification, diagnosis and clinical manifestations of apical periodontitis. *Endodontic Topics* **8**, 36-54 (2004).
18. Lee, J.H., Kim, D.H., Jeong, S.N., Choi, S.H. Detection and diagnosis of dental caries using a deep learning-based convolutional neural network algorithm. *J. Dent.* **77**, 106-11 (2018).
19. Lee, J.H., Kim, D.H., Jeong, S.N., Choi, S.H. Diagnosis and prediction of periodontally compromised teeth using a deep learning-based convolutional neural network algorithm. *J. Perio. Imp. Sci.* **48**, 114-123 (2018).
20. DeVries, T., Taylor, G.W. Dataset Augmentation in Feature Space. Preprint at https://arxiv.org/abs/1702.05538 (2017).

21. Shorten, C., Khoshgoftaar, T.M. A survey on Image Data Augmentation for Deep Learning. *J Big Data* **6,** 60 (2019).
22. Tang, Z. et al. OnlineAugment: Online Data Augmentation with Less Domain Knowledge. *European Conference on Computer Vision (ECCV)* **12352**; https://doi.org/10.1007/978-3-030-58571-6_19 (2020).
23. Zoph, B., Cubuk, E.D., Ghiasi, G., Lin, T.Y., Shlens, J., Le, Q.V. Learning Data Augmentation Strategies for Object Detection. *European Conference on Computer Vision (ECCV)* **12372**; https://doi.org/10.1007/978-3-030-58583-9_34 (2020).
24. Ronneberger, O., Fischer, P., Brox, T. U-Net: Convolutional Networks for Biomedical Image Segmentation. *Medical Image Computing and Computer-Assisted Intervention (MICCAI)* **9351**; https://doi.org/10.1007/978-3-319-24574-4_28 (2015).
25. Seferbekov, S., Iglovikov, V., Buslaev, A., Shvets, A. Feature Pyramid Network for Multi-Class Land Segmentation. *Proceedings of the IEEE Conference on Computer Vision and Pattern Recognition (CVPR)* 272-275 (2018).
26. Tompson, J., Goroshin, R., Jain, A., LeCun, Y., Bregler, C. Efficient object localization using convolutional networks. *Proceedings of the IEEE Conference on Computer Vision and Pattern Recognition (CVPR)* 648-656 (2015).

Figures

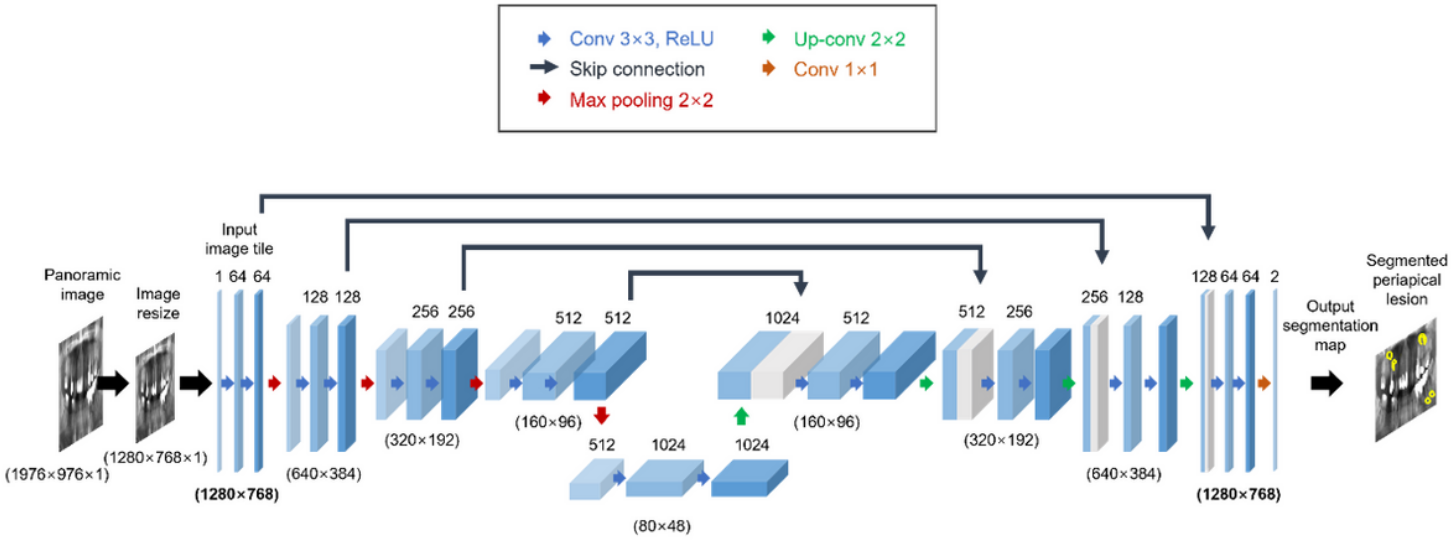

Figure 1

U-Net modelling architecture for detection apical lesion (example for 32x32 pixels in the lowest resolution). Each blue box represents a multi-channel feature map. The number of channels is labeled on top of the box. The x-y-size is offered at the bottom of the box. White boxes represent duplicated feature maps. The arrows indicate the different operations.

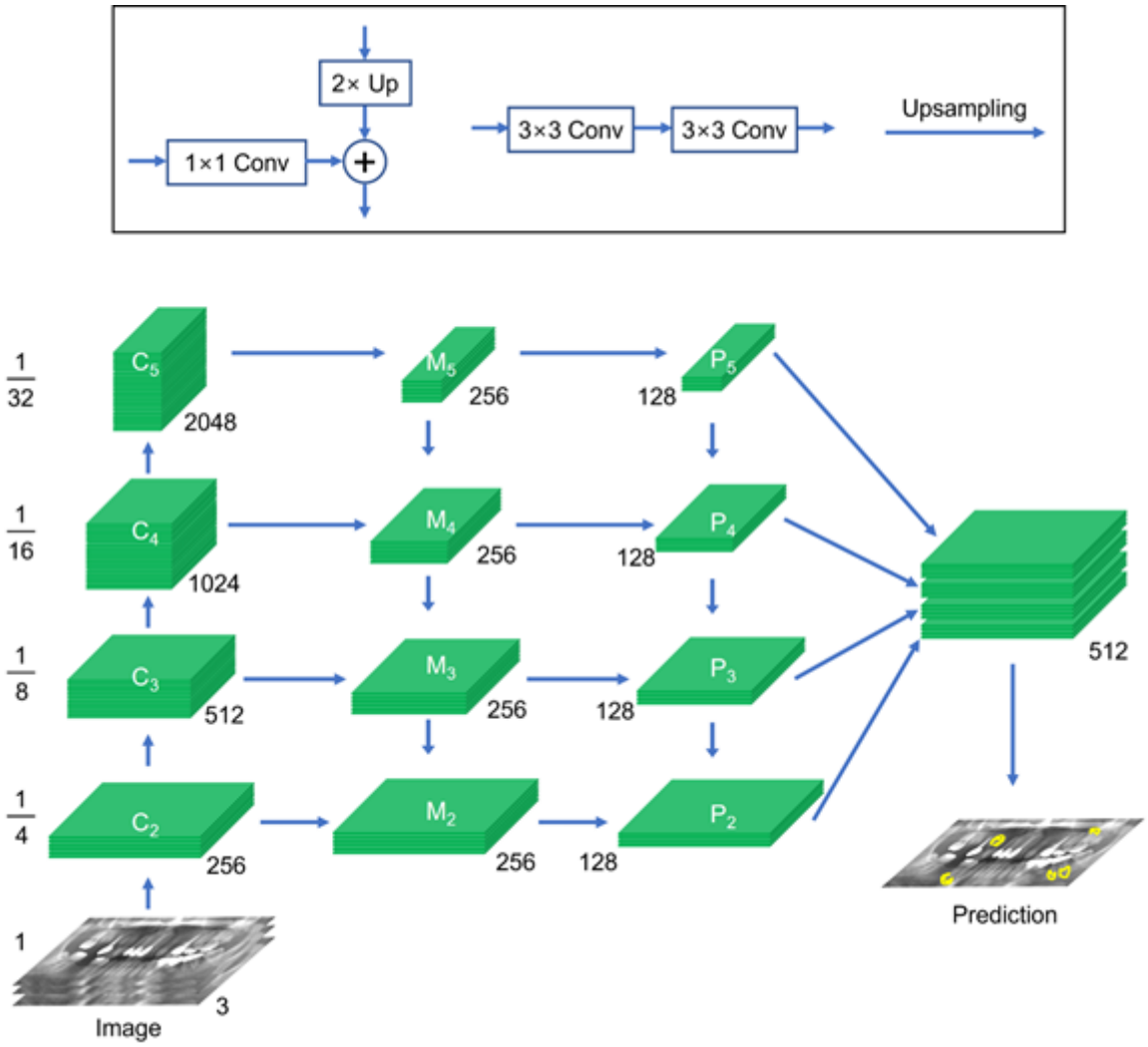

Figure 2

Feature pyramid network with Resnet50 encoder. The number of channels increases step-by-step on the left part of the scheme while the size of the feature maps decreases step-by-step. The arrows on top denote transformations implemented between the layers. In the last step, feature maps upsample to the same size and combined. The number of channels is decreased to the number of classes, and the output image is upsampled to the original image size.

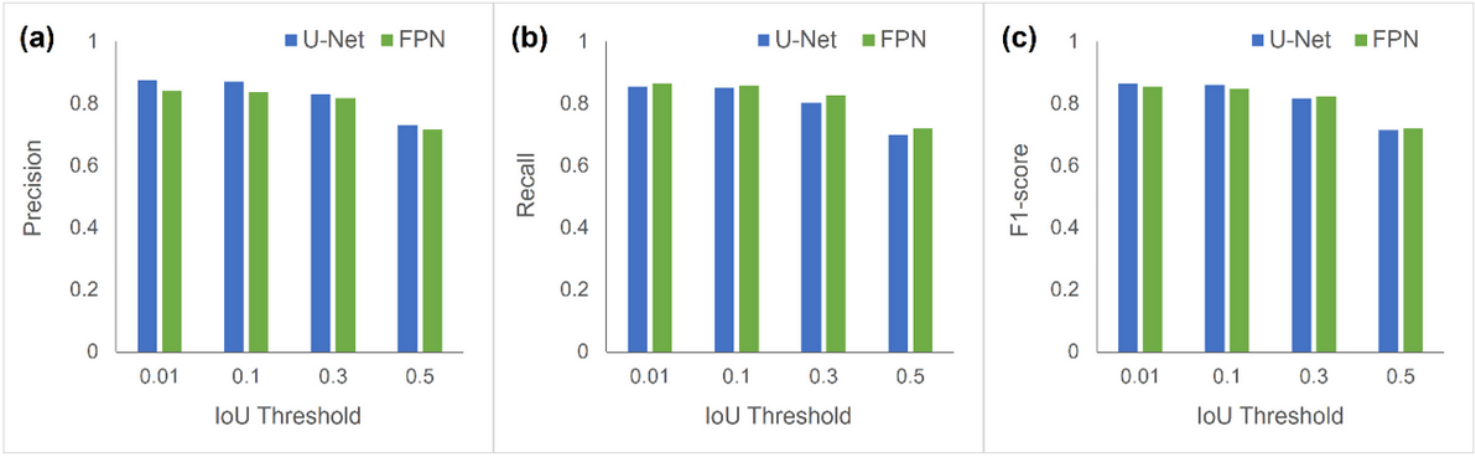

Figure 3

Comparison of U-Net and FPN with respect to detecting performances including precision (a), recall (b), and F1-score (c). Both models showed great performances for detecting the apical lesions, but U-Net showed slightly greater performance at 0.01 IoU value for F1-score.

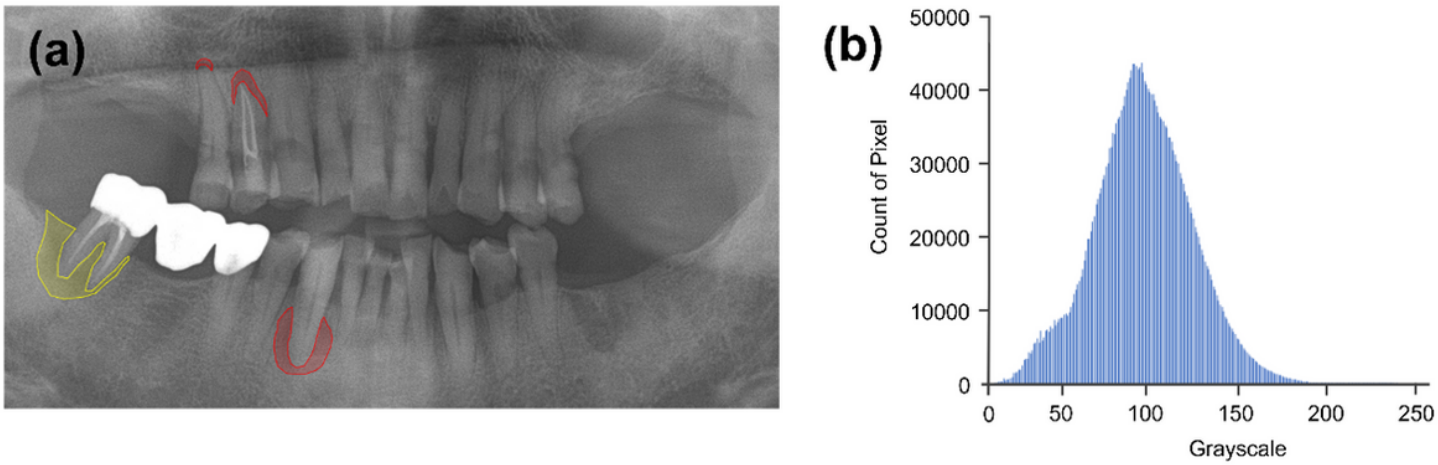

Figure 4

Lesions are labeled by outlining with the polygon labeling tools in training software called ‘deep stack’. Apical lesions are labeled in red and endodontic-periodontic lesions are labeled in yellow (a). Intensity histogram shows overall consistency without jagged edges in a specific labeled lesion (b).

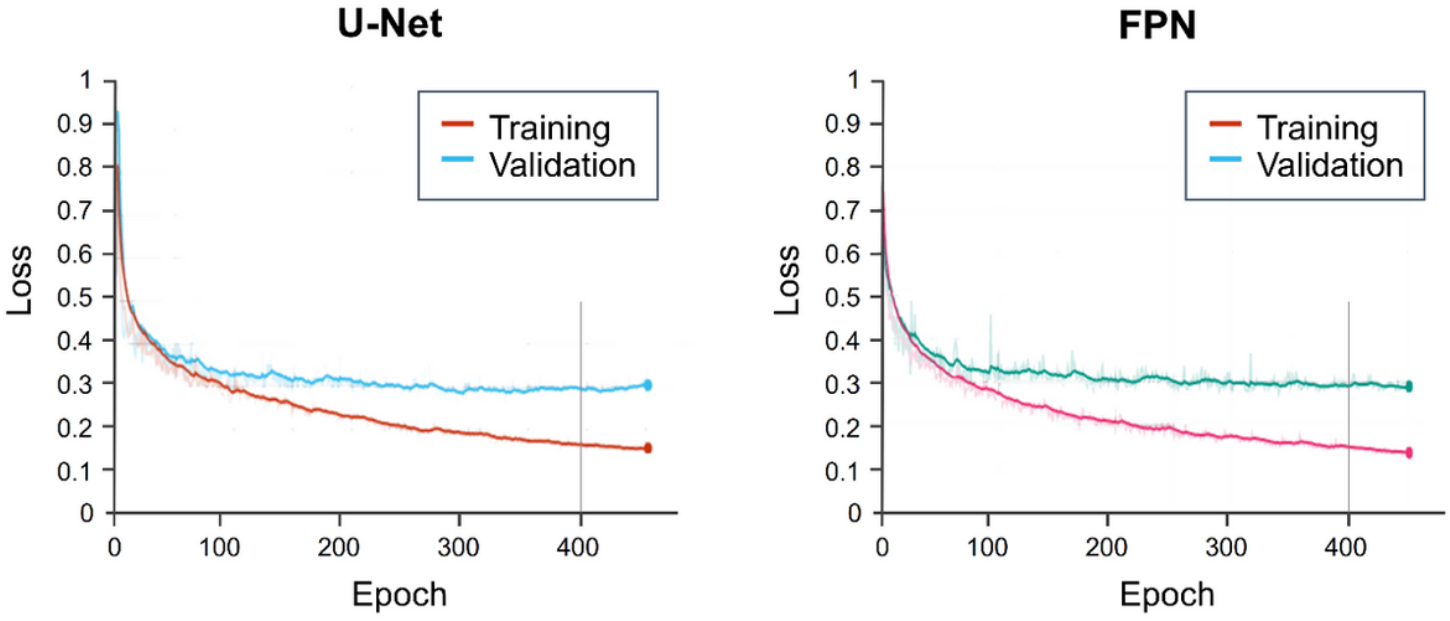

Figure 5

Comparison of the training and validation curves for the pretrained augmented models based on U-Net and FPN. Training and validation were performed for 450 epochs with each epoch representing one pass through the entire training and validation dataset. Overfitting was minimized under 400 epochs.

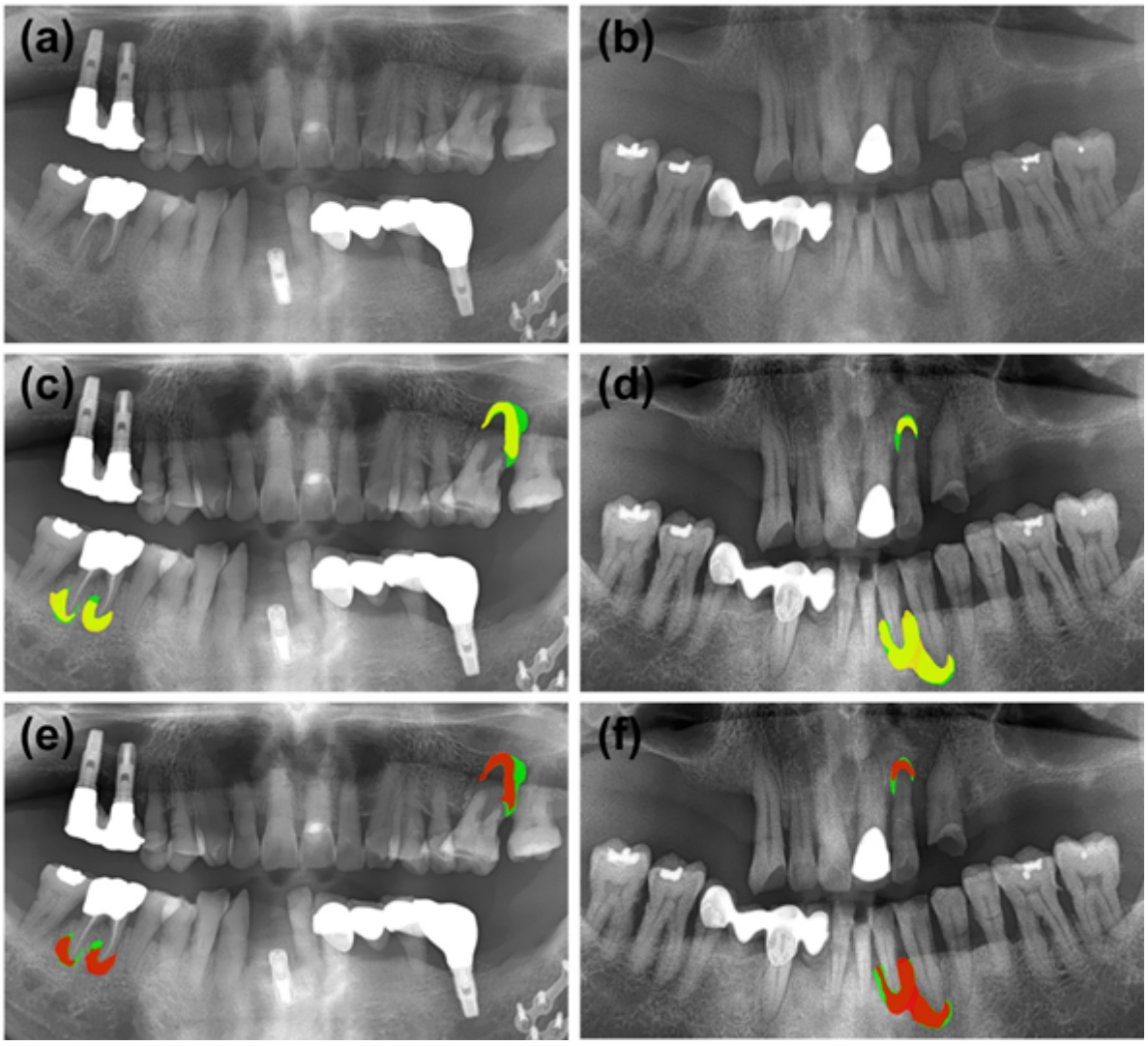

Figure 6

Results of apical lesion segmentation from panoramic radiographs using U-Net and FPN. Original panoramic radiographs were prepared for training (a,b). The green areas denote the manual labeling. The yellow areas denote the U-Net model-generated areas (c,d) and the red areas denote the FPN model-generated areas (e,f), respectively.